

# Hydrogen Forms in Water by Proton Transfer to a Distorted Electron

Ondrej Marsalek,<sup>†,||</sup> Tomaso Frigato,<sup>‡,||</sup> Joost VandeVondele,<sup>§</sup> Stephen E. Bradforth,<sup>⊥</sup>  
Burkhard Schmidt,<sup>‡</sup> Christof Schütte,<sup>‡</sup> and Pavel Jungwirth<sup>\*,†</sup>

*Institute of Organic Chemistry and Biochemistry, Academy of Sciences of the Czech Republic and Center for Biomolecules and Complex Molecular Systems, Flemingovo nám. 2, 16610 Prague 6, Czech Republic, Institut für Mathematik, Freie Universität Berlin, Arnimallee 6, D-14195, Berlin, Germany, Physical Chemistry Institute, Zürich University, Winterthurerstrasse 190, CH-8057 Zürich, Switzerland, and Department of Chemistry, University of Southern California, Los Angeles, California 90089-0482, U.S.A.*

*Received: September 17, 2009; Revised Manuscript Received: October 29, 2009*

Solvated electrons are ubiquitous intermediates in radiation-induced processes, with their lifetime being determined by quenching processes, such as the direct reaction with protons under acidic conditions. Ab initio molecular dynamics simulations allow us to unravel with molecular resolution the ultrafast reaction mechanism by which the electron and proton react in water. The path to a successful reaction involves a distortion and contraction of the hydrated electron and a rapid proton motion along a chain of hydrogen bonds, terminating on the water molecule most protruding into the electron cloud. This fundamental reaction is thus decidedly shown to be of a proton-transfer rather than electron-transfer character. Due to the desolvation penalty connected with breaking of the hydration shells of these charged particles, the reaction is, however, not diffusion-limited, in agreement with the interpretation of kinetics measurements.

## Introduction

Solvated electrons are formed when high-energy radiation passes through condensed material ranging from biological tissue to polymers, ceramics, or aqueous solutions used for nuclear waste storage and reprocessing. Water, in particular, has played a central role in radiation chemistry; understanding the chemical reactions that occur subsequent to the initial ionizing events is essential to model radiation-induced processes in the broader class of soft matter.<sup>1,2</sup> The electron in water polarizes the neighboring solvent molecules, creating a hydrated electron, which possesses a fluctuating structure with an average radius of gyration<sup>3,4</sup> of about 2.5 Å. When water is ionized, electrons are hydrated on a time scale shorter than 1 ps, and these species are highly reducing.<sup>1,2</sup> In pure deoxygenated water, the electron can survive for milliseconds, but its reaction with either added quenchers or (bio)chemical systems already dissolved within the liquid are key to the nature of radiation damage that occurs subsequently.

Acids are often used to quench (or scavenge) solvated electrons. For example, the proton quenching reaction plays an important role in the highly acidic media used for reprocessing spent nuclear material (PUREX process). Despite this ubiquitous role of quenching reactions in the radiation chemistry of aqueous systems and the fact that the kinetics of such quenching reactions have been known for decades,<sup>5</sup> a molecular picture for the mechanism of this intriguing class of fundamental reactions has remained elusive.

The electron–proton reaction leading to a hydrogen atom is seemingly the most elementary chemical process, at least in the

gas phase, where 1312 kJ mol<sup>−1</sup> are released upon association. In water, the strong solvation of both charged particles substantially reduces the exoergicity ( $\Delta G_{298}^\circ = -50$  kJ mol<sup>−1</sup>), and the reaction mechanism becomes correspondingly much more complex.<sup>6</sup> The reaction can be thought of as either a proton transfer from a hydronium ion to a weak base, forming the H atom in the former cavity of the electron,<sup>7,8</sup> or an electron transfer onto H<sub>3</sub>O<sup>+</sup>, forming transiently H<sub>3</sub>O, which rapidly dissociates.<sup>5</sup> There has been considerable argument over which is the correct picture.<sup>5,7,8</sup> In either case, the process is a reaction between an aqueous H<sub>3</sub>O<sup>+</sup> and a water shell polarized around a central negatively charged cavity of e<sub>aq</sub><sup>−</sup>. It is the subtle way in which the solvent shells need to respond to the motion of each particle that holds the key to understanding the reaction mechanism. The reaction is fast ( $k_{298} = 2.3 \times 10^{10}$  M<sup>−1</sup> s<sup>−1</sup>).<sup>5,9,10</sup> However, compared to the H<sup>+</sup> + OH<sup>−</sup> → H<sub>2</sub>O reaction, which similarly requires a large solvent rearrangement upon the loss of two ionic hydration shells, the electron–proton reaction in water is almost an order of magnitude slower.<sup>2</sup> Furthermore, despite the Coulomb attraction and the high mobility of H<sup>+</sup>, the electron–proton reaction is slower than either of the H + e<sub>aq</sub><sup>−</sup> + H<sub>2</sub>O → H<sub>2</sub> + OH<sup>−</sup> or OH + e<sub>aq</sub><sup>−</sup> → OH<sup>−</sup> reactions.<sup>2</sup> The comparison with the latter is significant since most solvated electrons produced in the ionization of water recombine with the geminate OH rather than the geminate hydronium.<sup>11,12</sup> Analysis of kinetic studies<sup>6</sup> suggests a barrier to the “contact” reaction of the electron–proton pair with passage time of ~20 ps.

Although the solvated electron as an unusual quantum solute has been an attractive target for nonlinear spectroscopy in the liquid-phase and gas-phase spectroscopy of anionic water clusters, the reactivity of solvated electrons has mainly been charted by pulse radiolysis pump–probe spectroscopy.<sup>1</sup> On the theory side, calculations have dealt with the equilibrium structure and spectroscopy of the hydrated electron,<sup>4,13–17</sup> with its reaction with a proton addressed previously only with static calculations

\* To whom correspondence should be addressed. E-mail: pavel.jungwirth@uochb.cas.cz. Fax: +420 220 410 320.

<sup>†</sup> Academy of Sciences of the Czech Republic and Center for Biomolecules and Complex Molecular Systems.

<sup>‡</sup> Freie Universität Berlin.

<sup>§</sup> Zürich University.

<sup>⊥</sup> University of Southern California.

<sup>||</sup> Both authors contributed equally.

for a small model system of an isolated Eigen cation ( $\text{H}_9\text{O}_4^+$ ).<sup>18</sup> The dynamical simulations reported here thus represent the first successful modeling of the quenching reaction of the hydrated electron in a system already possessing features pertinent to bulk water, using the full power of methods that compute the electronic structure as it evolves in time.

## Methods Section

This section provides computational details pertinent to the present *ab initio* MD simulations of reactive quenching of the hydrated electron by an excess proton. A set of 10 independent initial conditions were prepared using a 500 ps classical molecular dynamics run of a water cluster containing 31  $\text{H}_2\text{O}$  molecules and a single hydronium ( $\text{H}_3\text{O}^+$ ) and the electron substituted by a negative ion of comparable size.<sup>17</sup> At  $t = 0$ , we switched to *ab initio* MD, simulating nominally a  $\text{H}^+\text{e}^-(\text{H}_2\text{O})_{32}$  system at the same geometry, employing the semilocal Perdew–Burke–Ernzerhof exchange–correlation functional empirically corrected for long-range dispersion interactions.<sup>19</sup> The Goedecker–Teter–Hutter norm-conserving pseudopotentials<sup>20</sup> replaced the oxygen core electrons. The Kohn–Sham orbitals were expanded in an atom-centered triple- $\zeta$  Gaussian basis set augmented with two polarization functions and additional diffuse functions<sup>21</sup> that are necessary for proper description of the solvated electron. The use of the restricted open-shell formalism allowed us to employ the self-interaction correction (SIC) for the unpaired electron.<sup>22</sup> Only with the use of the SIC do the results compare quantitatively to benchmark MP2 calculations.

The optimal values of the SIC parameters  $a$  and  $b$  were obtained by minimizing the mean-square difference (MSD) between SIC-DFT and RI-UMP2/aug-cc-pVDZ energies for geometries sampled along two different reactive trajectories. A total of 17 configurations were employed, and for each trajectory, energies were shifted to zero average before computing the MSD. The optimization procedure yielded the following values of the SIC parameters:  $a = 0.313$  and  $b = 0.180$ . These were subsequently rounded to  $a = 0.3$  and  $b = 0.2$  as it was found that around these values, the choice of SIC parameters influenced only slightly the calculated energies. Note that comparing DFT calculations with and without SIC showed that the latter shifts up the energy of the reaction product (i.e., the H atom) with respect to the reactants by up to 80 kJ/mol, hindering therefore the recombination process.

The convergence of the employed basis set in terms of the description of the hydrated electron was checked by augmenting the m-TZVP basis set<sup>23</sup> by diffuse Gaussian functions with an exponent of 0.1 distributed uniformly in space on a cubic grid with a lattice constant of 2 Å. Tests for one of the reactive trajectories show that this has only a minor effect of a relative stabilization of the reactants with respect to the products by about 30 kJ/mol (as compared to the basis set employed throughout the present study).

The system was placed in a  $20 \times 20 \times 20 \text{ Å}^3$  cubic box, and a cutoff of 280 Ry was used for the auxiliary plane wave basis set. The Poisson equation was treated with a wavelet-based solver with open boundary conditions, which are adequate for the investigated isolated system. Classical equations of motion were integrated with a time step of 0.5 fs within the microcanonical ensemble. Forces were obtained from an electronic structure calculation fully converged at each step. All dynamical calculations were performed using the CP2K package and its electronic structure module Quickstep,<sup>21</sup> employing a setup similar to that of our previous study that focused solely on the nonreactive behavior of the hydrated electron.<sup>17</sup>

The initial geometries for the presented simulations were obtained from classical molecular dynamics using an empirical force field. The system consisted of a cluster of 31 SPCE water molecules, a hydronium, and an iodide ion. For initiating each of the *ab initio* molecular dynamics simulations, we took a particular geometry along the classical trajectory, removed the iodide, and set the total charge of the system to 0. In this way, an initial cavity was created that is suitable for the solvated electron due to its size and polarization of the surrounding water molecules. Due to the presence of the proton, the electron does not exhibit such a strong tendency to drift fast to the surface via a delocalized state as in our previous study concerned with its nonreactive behavior (i.e., without the presence of the quenching proton).<sup>17</sup>

Finally, we provide here definitions of physical observables monitored during the simulations. The total spin density of the system is defined as the difference between electron densities of the two spin components

$$s(\mathbf{r}) = \rho_\alpha(\mathbf{r}) - \rho_\beta(\mathbf{r}) \quad (1)$$

Because of the restricted open-shell formalism used in the present work, the spin density actually coincides with the electron density of the singly occupied Kohn–Sham orbital

$$s(\mathbf{r}) = \phi_{\text{SO}}(\mathbf{r})\phi_{\text{SO}}^*(\mathbf{r}) \quad (2)$$

In the following, we work with a spin density normalized so that

$$\int s(\mathbf{r})d^3r = 1 \quad (3)$$

From this spin density, further quantities are derived. The center of the spin density (i.e., the position of the electron) is the first moment of the distribution

$$\mathbf{r}_c = \int \mathbf{r}s(\mathbf{r})d^3r \quad (4)$$

The radial distribution of the spin density relative to this center is then

$$4\pi r^2 s(R) = \int s(\mathbf{r} - \mathbf{r}_c)d\Omega \quad (5)$$

where  $R = |\mathbf{r} - \mathbf{r}_c|$  and  $d\Omega$  denotes an integration over the angular variables. The second moment of the distribution is the gyration tensor, given by

$$\mathbf{S} = \int (\mathbf{r} - \mathbf{r}_c)(\mathbf{r} - \mathbf{r}_c)s(\mathbf{r})d^3r \quad (6)$$

We denote the eigenvalues of this tensor as  $s_x^2$ ,  $s_y^2$ , and  $s_z^2$ . The relative shape anisotropy,  $\kappa^2$ , is defined in terms of these eigenvalues in a standard way.<sup>24</sup>

For the excess proton, we use the following definition. First, two closest protons are assigned to each oxygen atom, forming a water molecule. Then, the excess proton is identified as the one left after this assignment. As a consequence, in  $\text{H}_3\text{O}^+$ , the excess proton is the one connected to the central oxygen by the longest of the three O–H bonds. Note that due to this

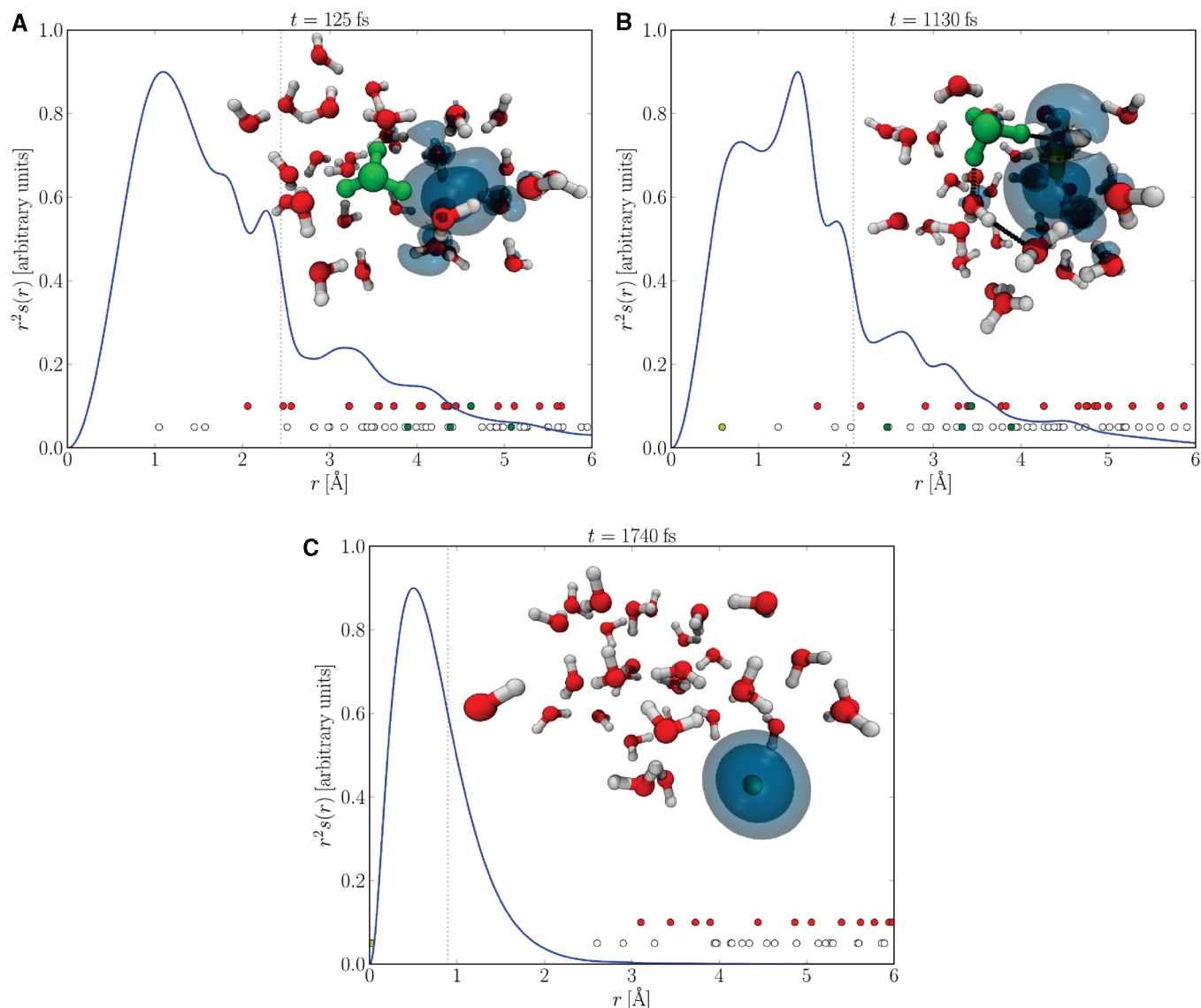


**Figure 1.** Electron distributions (spin densities) and snapshots of the system before (A), during (B), and after (C) the electron–proton reactive event. The vertical dotted line denotes the radius of gyration of the electron. White and red dots depict positions of water hydrogens and oxygens with respect to the electron, while the green color is used to label the atoms forming the hydronium cation. The single water hydrogen penetrating deep into the electron density just before the reaction and eventually becoming the product hydrogen atom is depicted in yellow in (B) and (C). The dashed black line in (B) highlights the hopping path of the proton along the chain of hydrogen-bonded water molecules prior to the reaction.

definition, the identity of the excess proton in  $\text{H}_3\text{O}^+$  can change during vibrational motions of this ion.

## Results

We chose a medium-sized cluster since it not only bears many similarities to the aqueous bulk but also allows for comparison to the extensive body of experimental data on photoionization and vibrational spectroscopy in electron-containing water clusters.<sup>25–27</sup> The present system with 32 water molecules is large enough to possess an interior region, in which the solvated electron initially resides in a pre-existing polarized cavity (see Figure 1A and Methods Section for details). At the same time, we can take advantage of the finite size of the system in the sense that it reduces the phase space that the excess proton, initially bound to a water molecule well separated from this cavity (Figure 1A), has to explore before the reaction. Another fact that makes the reaction more feasible in the cluster is the slightly lower binding energy of the electron,<sup>17</sup> which effectively destabilizes the reactants with respect to the products and thus

accelerates the process. In summary, the reaction in the present cluster is a good proxy to that in the aqueous bulk, being at the same time computationally more accessible.

We obtained a total of 10 *ab initio* molecular dynamics (MD) trajectories, each propagated for several picoseconds (for computational details, see the Methods Section and for animations see the Supporting Information). Three of these trajectories captured a successful reaction event leading to formation of a hydrogen atom within 1–3.5 ps, while for the other seven trajectories, the reaction did not occur over this time scale. The reaction is most usefully described and quantified by analyzing these trajectories in terms of the concerted dynamical behavior of the excess proton and the hydrated electron. The three frames in Figure 1 depict for one of the reactive trajectories the excess electron (i.e., the total spin density) radial distribution function, together with snapshots taken before, at the moment of, and after the electron–proton reactive event. Before the reaction, the excess electron is localized from roughly 80%<sup>15,16</sup> in the polarized water cavity, with the remainder of its spin density

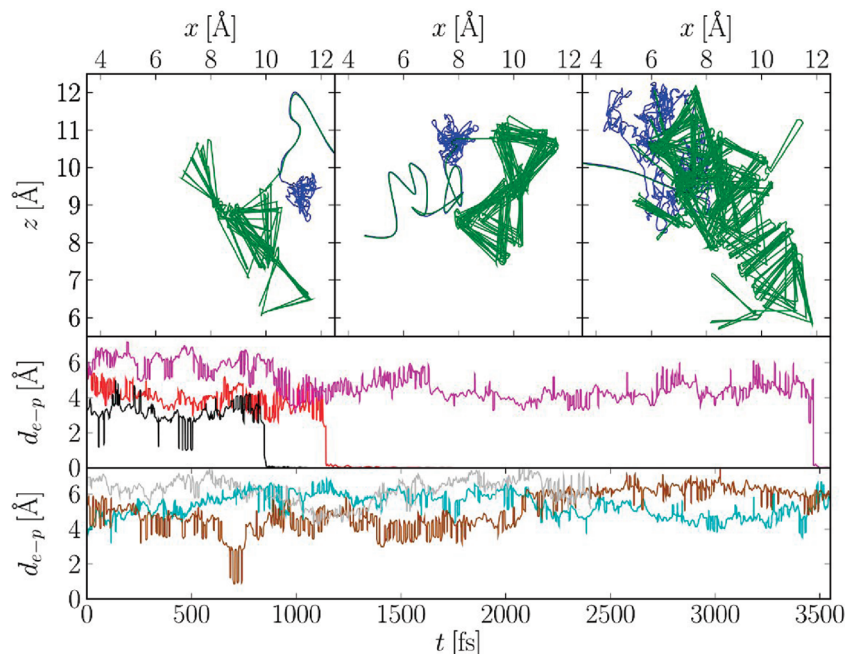


**Figure 2.** Projections of the electron (blue) and proton (green) trajectories on the  $xz$ -plane for the three reactive trajectories (upper panels) and time evolution of the mutual separation of the excess proton and the center of mass of the hydrated electron for three reactive (middle panel: black, red, and violet) and three nonreactive (bottom panel: brown, cyan, and gray) trajectories. The projections show that the electron smoothly diffuses within the system while the proton is more mobile, exhibiting frequent hops (note that the triangular parts of the trajectories correspond to shuffling of the excess proton within a single water molecule). These projections, together with plots showing that the electron–proton separation does not decrease until just before the reactive event (or attempts thereof), illustrate that the reaction is not diffusion-limited.

being distributed over the neighboring solvent molecules (Figure 1A). The cavity is spherical only on average, with large instantaneous fluctuations of its shape and size. Right before the reaction, the electron spin density changes shape, remaining elongated in the direction of a particularly strongly solvating water molecule (Figure 1B). The excess proton moves to this molecule, reacting with the electron and forming a hydrogen atom (Figure 1C).

The motion of the excess proton is qualitatively different from that of the hydrated electron. While the electron constantly reshapes but diffuses relatively slowly<sup>28</sup> within the system, the proton moves faster by a hopping mechanism.<sup>29,30</sup> Note that the excess proton is defined as the one that remains after each oxygen atom is assigned the two hydrogens nearest to it. This proton is then depicted as chemically bound to its nearest water molecule (Figure 1). Before the reaction, the identity of this excess proton changes frequently within a single hydronium, which makes it available for occasional proton transfer to neighboring water molecules.<sup>30</sup> The present classical description of nuclear motions provides a qualitatively correct description of the proton motion,<sup>31</sup> which can be further enhanced if quantum nuclear effects such as tunneling are taken into account.<sup>32</sup>

The relative motion of the two reactants in all three reactive trajectories, as well as in three representative unreactive trajectories, is demonstrated in Figure 2 (lower two panels), which plots the time evolution of the mutual separation of the proton and the center of the electron density. The upper panels of Figure 2 show for the reactive events a projection of the electron and proton trajectories onto the  $xz$ -plane. Figure 2 clearly demonstrates that the proton with its frequent hops is the “light” particle while the electron due to its relatively strongly bound solvent shell is the “heavy” one, which represents an interesting but understandable reversal of the usual roles of the electron and proton.

The reaction occurs only after many proton hops along the hydrogen-bonded chain of water molecules and several unsuccessful attempts at reacting with the electron (see Figures 2 and 3). The electron–proton reaction is thus not a diffusion-limited process since direct association of electron and proton into a hydrogen atom in water is hindered by the desolvation penalty of the two charged reactants. The sequence of events leading to the reaction is further illustrated by Figure 3, which presents (for the reactive trajectory shown in Figure 1) the time evolution of the mean sizes of the electron spin density along the three principal axes of its gyration tensor. Initially, the electron is roughly spherical; however, each attempt at reaction (marked by a decrease in electron size) is accompanied by its distortion toward a prolate shape. This can be understood in terms of an asymmetric solvation shell, with one or two water molecules penetrating deeper into the electronic cloud, being more reactive than a symmetric one. A successful reactive event is thus accompanied by a dramatic change from (on average) a spherical to a prolate shape of the electron density, after which the electron shrinks to the size of a hydrogen atom, becoming almost a perfect sphere. This effect is further exemplified in Figure 4, which shows for the three reactive trajectories the correlation between the radius of gyration and asymmetry of the electron. Note the anisotropic compression in two dimensions of the electron density occurring in the early stages of the electron–proton reaction. The electron distortion is, to a large extent, driven by the reacting proton. This also follows from comparison with previous simulations of an electron (without a proton) in a water cluster of the same size, where no such large asymmetries of the electron density were observed.<sup>17</sup>

## Discussion

The fact that only 3 out of 10 trajectories led to a successful reaction emphasizes that the reactants do not simply diffuse



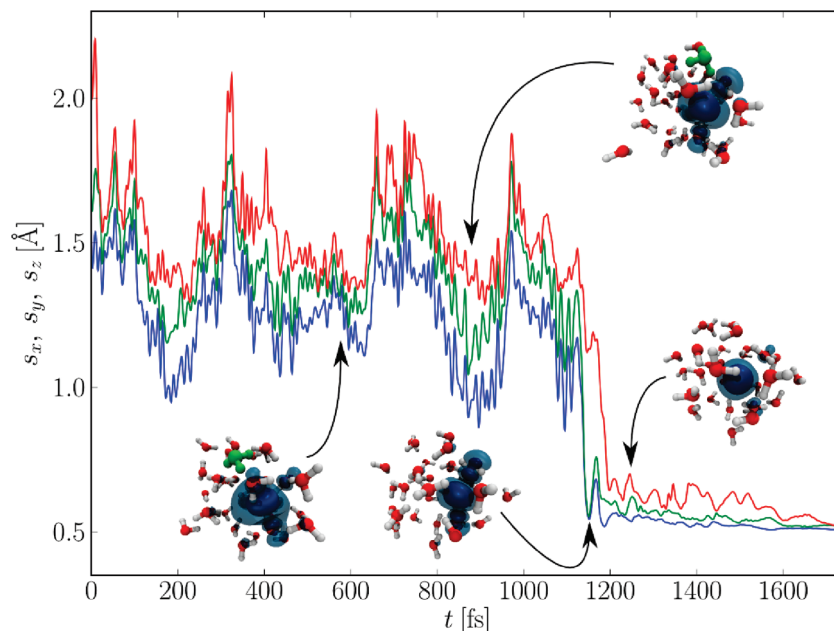


**Figure 3.** Time evolution of the square roots of the principal moments of the gyration tensor of the excess electron taken from one trajectory, characterizing the size and asymmetry of its distribution, together with representative snapshots of the system. Note the correlation between increased asymmetry, characterized by large differences between the three eigenvalues, and the tendency of the electron to react with the proton.

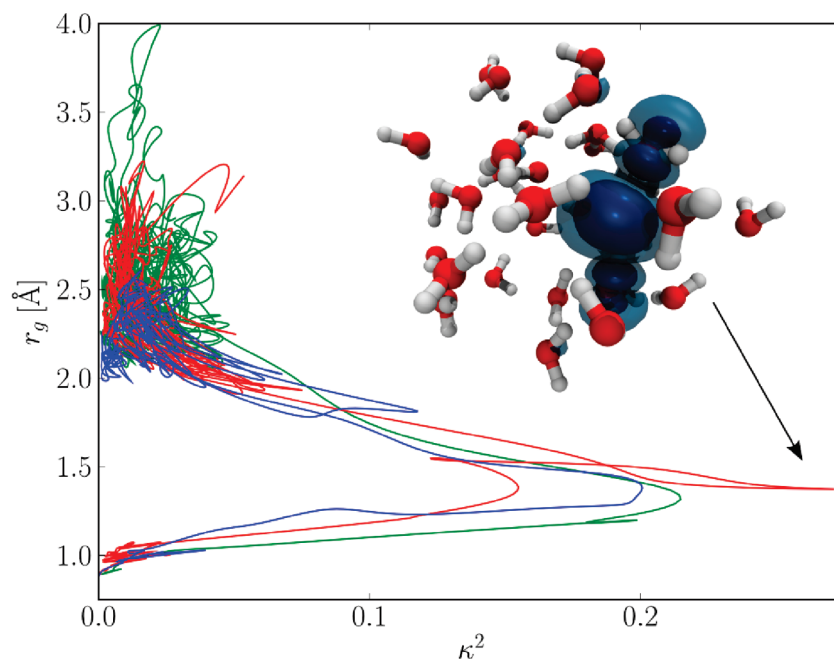


**Figure 4.** Correlation between the radius of gyration,  $r_g$ , and the relative shape anisotropy,  $\kappa^2$ , for the three reactive trajectories. Note the reactant basin of the hydrated electron (large radius and small asymmetry) connected with the product basin of the hydrogen atom (small radius and small asymmetry) via a transition structure (also shown as a snapshot) with an intermediate radius and large asymmetry.

toward each other and react, in which case the reaction would always occur in the simulated water cluster within several hundred femtoseconds. The reason for the slow-down of the reaction is that not only are two hydration shells around charged species lost but also the product H atom is hydrophobic, so there is a very large solvent rearrangement penalty. This picture of a barrier to reaction is fully consistent with the interpretation of the bulk experimental rate constant and its temperature dependence; namely, the reaction is only partially diffusion-controlled at all temperatures measured,<sup>6</sup> and the diffusion-limited rate would be at least 5 times higher at room temperature<sup>2,6,12</sup> (vide infra).

As expected from dielectric continuum theories, the room-temperature bimolecular rate constant decreases markedly from  $2.3 \times 10^{10} \text{ M}^{-1} \text{ s}^{-12}$  upon going to high ionic strength due to screening of the attractive Coulomb attraction between the reactants. The ionic strength dependence in quenching reactions, including this one, was the original evidence used to establish the solvated electron as the main reducing species produced by radiolysis by virtue of its charge.<sup>34</sup>

Although the number of trajectories computed here is not sufficient to predict a reaction rate for the cluster, simple use of the bulk rate constant adjusted for ionic strength,<sup>2,10</sup> along with the effective  $\text{H}_3\text{O}^+$  concentration in the cluster suggests

an average reaction time of  $\sim 50$  ps.<sup>35</sup> The fact that only 30% of our trajectories have reacted over 3.5 ps indicates that the present ab initio MD methodology is semiquantitative in describing the reaction.

The quenching reaction by protons of the solvated electron has been investigated for at least 50 years due to its significance in condensed-phase radiation chemistry. From the thermodynamic and kinetic data established for this reaction, many significant mechanistic insights have been gained, although as mentioned in the Introduction, there have been long-standing arguments as to whether the electron moves onto the hydronium ion or whether the electron accepts a proton. The atomistic picture developed in the current work helps to amplify many of the kinetic observations and clarify the primary mechanism.

This electron–proton reaction in water is widely agreed not to be under diffusion control.<sup>5,6,9</sup> The  $\sim 11$  kJ mol<sup>−1</sup> activation energy is very close to the activation energy connected with the diffusion coefficient in water. However, Shiraishi and others have shown that, based on a Debye–Smoluchowski estimate, the rate is lower than the diffusion limit by a factor of 5–10 over a large range of temperatures.<sup>6</sup> The kinetic isotopic effect for the reaction is relatively large. Direct measurements in relatively concentrated acid solution show almost a factor of 2 slower bimolecular rate constant for D<sub>2</sub>O.<sup>33</sup> This evidence has been cited in the past to support an electron-transfer mechanism producing a H<sub>3</sub>O radical,<sup>5</sup> but substantial rearrangement of the solvent shell (as seen in the simulation here) has also been argued to explain the isotope effect in support of a proton-transfer mechanism.<sup>8</sup>

## Conclusions

The present simulations show that formation of hydrogen from an electron and proton in water is fundamentally a proton-transfer reaction and that there is no H<sub>3</sub>O intermediate. This differs from the assertion that the solvated electron always reacts by electron transfer,<sup>5</sup> which is found in most of the older, but still referenced, reviews and texts of the radiation chemistry field.<sup>2</sup> We are, however, in agreement with the more recent consensus<sup>8</sup> that in many solvated electron reactions with Brønsted acids, the electron is acting as a base.<sup>7</sup> The present ab initio MD simulations thus provide a detailed and contemporary picture of a token quenching process of a hydrated electron, that is, the electron–proton reaction in water, directly elucidating the molecular mechanism of this most fundamental process in radiation chemistry.

**Acknowledgment.** The authors thank David Bartels for valuable conversations about this reaction. Support from the Czech Science Foundation (Grants 203/08/0114) and the Czech Ministry of Education (Grant LC512) and is acknowledged. Part of the work in Prague was supported via Project Z40550506. O.M. acknowledges support from the International Max-Planck Research School for Dynamical Processes in Atoms, Molecules and Solids. S.E.B. thanks the U.S. National Science Foundation for support (CHE-0617060). T.F. acknowledges support from the Center of Scientific Simulations, FU Berlin. A part of the presented calculations has been performed on the HLRN supercomputer.

**Supporting Information Available:** Animations of the three reactive trajectories and details concerning these trajectories are

provided as Supporting Information. This material is available free of charge via the Internet at <http://pubs.acs.org>.

## References and Notes

- (1) Garrett, B. C.; Dixon, D. A.; Camaioni, D. M.; Chipman, D. M.; Johnson, M. A.; Jonah, C. D.; Kimmel, G. A.; Miller, J. H.; Rescigno, T. N.; Rossky, P. J.; Xantheas, S. S.; Colson, S. D.; Laufer, A. H.; Ray, D.; Barbara, P. F.; Bartels, D. M.; Becker, K. H.; Bowen, H.; Bradforth, S. E.; Carmichael, I.; Coe, J. V.; Corrales, L. R.; Cowin, J. P.; Dupuis, M.; Eiseenthal, K. B.; Franz, J. A.; Gutowski, M. S.; Jordan, K. D.; Kay, B. D.; LaVerne, J. A.; Lyman, S. V.; Madey, T. E.; McCurdy, C. W.; Meisel, D.; Mukamel, S.; Nilsson, A. R.; Orlando, T. M.; Petrik, N. G.; Pimblott, S. M.; Rustad, J. R.; Schenter, G. K.; Singer, S. J.; Tokmakoff, A.; Wang, L. S.; Wittig, C.; Zwiernik, T. S. *Chem. Rev.* **2005**, *105*, 355.
- (2) Buxton, G. V.; Greenstock, C. L.; Helman, W. P.; Ross, A. B. *J. Phys. Chem. Ref. Data* **1988**, *17*, 513.
- (3) Bartels, D. M.; Takahashi, K.; Cline, J. A.; Marin, T. W.; Jonah, C. D. *J. Phys. Chem. A* **2005**, *109*, 1299.
- (4) Turi, L.; Sheu, W. S.; Rossky, P. J. *Science* **2005**, *309*, 914.
- (5) Hart, E.; Anbar, M. *The hydrated electron*; Wiley-Interscience: New York, 1970.
- (6) Shiraishi, H.; Sunaryo, G. R.; Ishigure, K. *J. Phys. Chem.* **1994**, *98*, 5164.
- (7) Stein, G. *Isr. J. Chem.* **1971**, *9*, 413.
- (8) Han, P.; Bartels, D. M. *J. Phys. Chem.* **1992**, *96*, 4899.
- (9) Barker, G. C.; Fowles, P.; Sammon, D. C.; Stringer, B. *Trans. Faraday Soc.* **1970**, *66*, 1498.
- (10) Kloepper, J. A.; Vilchiz, V. H.; Lenchenkov, V. A.; Chen, X. Y.; Bradforth, S. E. *J. Chem. Phys.* **2002**, *117*, 766.
- (11) Thomsen, C. L.; Madsen, D.; Keiding, S. R.; Thøgersen, J.; Christiansen, O. *J. Chem. Phys.* **1999**, *110*, 3453.
- (12) Goulet, T.; Jay-Gerin, J. P. *J. Chem. Phys.* **1992**, *96*, 5076.
- (13) Boero, M. *J. Phys. Chem. A* **2007**, *111*, 12248.
- (14) Barnett, R. N.; Landman, U.; Scharf, D.; Jortner, J. *Acc. Chem. Res.* **1989**, *22*, 350.
- (15) Shkrob, I. A. *J. Phys. Chem. A* **2007**, *111*, 5223.
- (16) Shkrob, I. A.; Glover, W. J.; Larsen, R. E.; Schwartz, B. J. *J. Phys. Chem. A* **2007**, *111*, 5232.
- (17) Frigato, T.; VandeVondele, J.; Schmidt, B.; Schutte, C.; Jungwirth, P. *J. Phys. Chem. A* **2008**, *112*, 6125.
- (18) Sobolewski, A. L.; Domcke, W. *Phys. Chem. Chem. Phys.* **2007**, *9*, 3818.
- (19) Grimme, S. *J. Comput. Chem.* **2006**, *27*, 1787.
- (20) Goedecker, S.; Teter, M.; Hutter, J. *Phys. Rev. B* **1996**, *54*, 1703.
- (21) VandeVondele, J.; Krack, M.; Mohamed, F.; Parrinello, M.; Chassaing, T.; Hutter, J. *Comput. Phys. Commun.* **2005**, *167*, 103.
- (22) VandeVondele, J.; Sprik, M. *Phys. Chem. Chem. Phys.* **2005**, *7*, 1363.
- (23) VandeVondele, J.; Hutter, J. *J. Chem. Phys.* **2007**, *127*, 114105.
- (24) Theodorou, D. N.; Suter, U. W. *Macromolecules* **1985**, *18*, 1206.
- (25) Lee, G. H.; Arnold, S. T.; Eaton, J. G.; Sarkas, H. W.; Bowen, K. H.; Ludewigt, C.; Haberland, H. Z. *Physik D: At., Mol. Clusters* **1991**, *20*, 9.
- (26) Verlet, J. R. R.; Bragg, A. E.; Kammrath, A.; Cheshnovsky, O.; Neumark, D. M. *Science* **2005**, *307*, 93.
- (27) Roscioli, J. R.; Hammer, N. I.; Johnson, M. A. *J. Phys. Chem. A* **2006**, *110*, 7517.
- (28) Schmidt, K. H.; Han, P.; Bartels, D. M. *J. Phys. Chem.* **1992**, *96*, 199.
- (29) Boero, M.; Ikeshoji, T.; Terakura, K. *ChemPhysChem* **2005**, *6*, 1775.
- (30) Marx, D.; Tuckerman, M. E.; Hutter, J.; Parrinello, M. *Nature* **1999**, *397*, 601.
- (31) Marx, D.; Tuckerman, M. E.; Parrinello, M. *J. Phys.: Condens. Matter* **2000**, *12*, A153.
- (32) Geissler, P. L.; Dellago, C.; Chandler, D.; Hutter, J.; Parrinello, M. *Science* **2001**, *291*, 2121.
- (33) Bartels, D. M.; Craw, M. T.; Han, P.; Trifunac, A. D. *J. Phys. Chem.* **1989**, *93*, 2412.
- (34) Czapski, G.; Schwarz, H. A. *J. Phys. Chem.* **1962**, *66*, 471.
- (35) In the system simulated here, with a single hydronium and 31 water molecules approximating the cluster as having the density of room-temperature water, the simulations would thus have  $\sim 1.8$  M ionic strength. The pseudo-first-order rate constant adjusted for ionic strength is  $(50 \text{ ps})^{-1}$  at  $[\text{H}_3\text{O}^+] = 1.8$  M. Following Shiraishi,<sup>6</sup> and assuming the cluster effectively has the two reactants in an “association complex”, we might alternatively predict a  $(26 \text{ ps})^{-1}$  rate for the reaction if it were to proceed as the bulk kinetics.